PROFILE RECONSTRUCTION TECHNIQUES FOR THE JET NEUTRON AND GAMMA-RAY CAMERAS

T. Craciunescu, I. Tiseanu, V. Zoita

National Institute of Laser, Plasma and Radiation Physics, Magurele

1. Overview

At the JET Tokamak a major goal is the production and measurement of high levels of neutron emission from d-d and d-t fusion reactions. A variety of neutron diagnostics are used independently at JET to measure both fast and thermal ion behavior. The available neutron diagnostics include a neutron profile monitor consisting of a vertical and horizontal camera. The JET neutron cameras, a unique instrument among similar diagnostics available at large fusion research facilities, consist of two concrete shields of which each includes a fan-shaped array of collimators. These collimators define a total of 19 lines of sight, grouped in two cameras (horizontal and vertical). The plasma coverage allows neutron the tomographic reconstruction of neutron emissivity spatial profiles in two dimensions. The reconstructions are useful for the study the thermal and beam-induced sources of neutron emission and to analyze the evolution of fast ion populations. However, due to the existence of only two fairly coarse views of the plasma, the tomographic problem is a highly limited data set one. This restricts the set of tomographic methods which can be used for the reconstruction.

A reconstruction method based on the maximum likelihood (ML) principle was developed for solving the reconstruction problem during the year 2008 [1]. In 2009 the main research topics were focuse on:

- Improvement, adaptation for JET tomographic geometry and implementation of several reconstruction methods - maximum entropy (ME), a Tikhonov regularization (TR) approach, and a Monte Carlo back-projection algorithm (MCBP).
- Assessment of the quality of the tomographic methods for reconstruction of neutron and gamma emissivity. Development of a comparative study.
- Diagnostics support in JET experimental campaigns based on tomographic validated methods.

The methods have been tested on numerically simulated phantoms with shapes characteristic for this kind of tomography. The retrieval of sophisticated structures in the emissive distribution has been addressed in order to have a complete image of the quality and reliability of the methods. A both qualitative and quantitative evaluation is reported. Extensive work was dedicated to the assessment of all the developed methods on pertinent experimental data sets.

The package of methods was used during the JET experimental campaigns. Diagnostics support, consisting in the reconstruction of the gamma emissivity distribution, was provided for fast ion studies. This demonstrated the usefulness of the package for inter-shot analysis.

In conclusion we appreciate that the objectives of the project were reached. A package of tomographic methods was developed, adapted and implemented for JET neutron and gamma tomography. The validation of the methods was performed both on neutronic and gamma-ray data. The methods were used to provide support in JET experimental campaigns. It allowed the retrieval of useful information needed during the experiments.

Publications

[1] T. Craciunescu, G. Bonheure, V. Kiptily, A. Murari, I. Tiseanu, V. Zoita*, A comparison of four reconstruction methods for JET neutron and gamma tomography*, Nuclear Inst. and Methods in Physics Research, A, 605, pp. 373-384, 2009

[2] V. G. Kiptily, C. P. Perez von Thun, S. D. Pinches, S. E. Sharapov, D. Borba, F. E. Cecil, D. Darrow, V. Goloborod'ko, T. Craciunescu, T. Johnson, F. Nabais, M. Reich, A. Salmi, V. Yavorskij, M. Cecconello, G. Gorini, P. Lomas, A. Murari, V. Parail , S. Popovichev, G. Saibene, R. Sartori, D.B. Syme, M. Tardocchi, P. de Vries, V.L. Zoita. *Recent progress in fast ion studies on JET*, Nuclear Fusion, 49, p. 065030, 2009.

[3] V.G. Kiptily, G. Gorini, I. Proverbio, M. Tardocchi, I.N. Chugunov, D. Gin, M. Nocente, S.D. Pinches, S.E. Sharapov, A.E. Shevelev, T. Craciunescu, F.E. Cecil, M. Gatu Johnson, V. Goloborod'ko, C. Hellesen, T. Johnson, K. Kneupner, A. Murari, P.G. Sanchez, D.B. Syme, P. de Vries, V. Yavorskij, V.L. Zoita, *Doppler Broadening of Gamma Ray Lines and Fast Ion Distribution in JET plasmas*, 11th IAEA Technical Meeting on Energetic Particles in Magnetic Confinement Systems, Kyiv, Ukraine.

2. Detailed results

2.1 Methods

In 2-D tomography systems, measurements are taken along lines of sight and can essentially be represented by line integrals; i.e. the measurement p is given by straight line integrals of the emissivity $f(x, y)$, where x and y are Cartesian coordinates of the plane. The emissivity function can be appropriately discretized on a 2-D grid. For this purpose, the reconstruction area is divided into pixels that are sufficiently small for emissivity variations within a pixel to be negligible. The weight matrix W describes the geometrical layout of the detectors and its element w_{ik} indicates the contribution of the ith pixel to the kth detector.

The basic set of tomographic equations is:

$$p_k = \sum_{i=1}^{N_p} w_{ik} \cdot f_i, \quad k = 1,2,...,N_d \tag{1}$$

where N_p and N_d are the numbers of pixels and detectors, respectively. As the tomographic problem is highly undetermined, the reconstruction algorithm can lead to a solution which satisfy Eq. 1 but has no physical relevance and may bring about wrong interpretations. A priori information about the expected emission profile can be introduced in order to compensate for the lack of experimental information. Smoothness can be imposed on the solution of the tomographic problem as regularization. In order to prevent over-smoothing which may lead to the blurring of certain features in the reconstruction, it is necessary to find the smoothest function for which the misfit is equal to the estimated noise. We used a smoothing operator defined in Ref. 1which is implemented as one-dimensional median filtering, using a sliding window which moves on the magnetic contour lines. This smoothing operator does not need to be integrated in the objective function of the tomographic problem. It works directly on the reconstructed image, at different stages of the reconstruction process. This technique was an appropriate choice for this work, which deals with a variety of methods with different algorithmic formulations. Additional smoothing can be obtained by resampling the experimental projection. Projection resampling implies the introducing of virtual lines of sight which ensures an improved coverage of the reconstruction domain.

2.1.1 Maximum likelihood

Bayesian statistics represents an appropriate framework for introducing the ML method. Bayesian inference provides a numerical measure of the probability of some event with consistent consideration for prior information. Bayes' theorem supplies the rule for determining the posterior probability:

$$P(f|p,z) = P(p|f,z)\frac{P(f|z)}{P(p|z)} \tag{2}$$

where f is a particular solution in view of experimental data p and additional parameters z (e.g. error bars). $P(p|f,z)$ quantifies the probability of measuring data p if a reconstruction f and parameters z are given. It represents the likelihood function, which contains the new information provided by the experiment. According to Bayes' theorem, the likelihood has to be blended with the prior probability $P(f|z)$ based on the information z prior to any experiment - of getting the posterior probability distribution. $P(p|z)$ is not related to the maximal value of $P(f|p,z)$ and so will be treated as a constant for the present purpose. The most trustworthy reconstruction is that which maximizes the probability distribution $P(f|p,z)$ (see Eq. (2)). If there is no a priori source information available, $P(f|z)$ can be assumed as constant, implying that all possible source distribution are equally likely, therefore maximizing the Bayesian results in the same way as maximum likelihood. In tomography problems, the likelihood probability density function follows the error statistics of the experimental data. If it is assumed that each projection ray p obeys Poisson statistics, with all of them statistically uncorrelated, the likelihood function $P(p|f,z)$ has the form:

$$P(p|f,z) = \prod_k \left[\frac{1}{p_k!}\left(\sum_i w_{ik} f_i\right)^{p_k} \times \exp\left(-\sum_i w_{ik} f_i\right)\right] \tag{3}$$

An efficient iterative solution of this nonlinear optimization problem was given in Refs. 2-3. The iterative ML algorithm works directly on the reconstructed image which is successively updated. This allows image manipulation, at each iteration, for introducing a priori knowledge. Therefore smoothing is applied, as described, at each iteration.

2.2.2 Maximum entropy

The maximum entropy (ME) has become a common regularization method and a widely adopted way to overcome the indeterminacy of ill-posed problems. ME can be derived starting also from the Bayes formula (2), by a different choice of the prior probability $P(f|z)$ and also of the likelihood function $P(p|f,z)$. The total lack of information about the emissive source assumed in the case of ML method is replaced by the simplest expert knowledge: the emissivity distribution have to be positive. Thus, within the Bayesian approach, this expert knowledge enters the analysis as prior distribution and contributes to the shape of the posterior distribution. On the basis of information theory, Skilling [4] have shown that the most uninformative and most unbiased prior is the entropic prior:

$$P(p|f,z) = {\frac{\alpha}{2\pi}}^{N_p/2} \exp(\alpha S) \tag{4}$$

where: $S = \sum_{i}^{N_p} \left[f_i - m_i - f_i \ln\left(\frac{f_i}{m_i}\right) \right]$ is the entropy relative to the default model m and α is a positive constant. The default model m is that reconstruction where the entropy and the prior have their maximum, and to which f would default in the absence of any data. Possible prior information about the structure of the solution can be encoded in the default model. However, the usual approach is to consider complete prior ignorance, which means a flat distribution for m ($m_i = const$). The entropic prior is a positive and additive distribution function.

The probability of obtaining a certain signal $p(f)$, with f given, is defined by the error statistics appropriate to the respective experimental problem. Most of the data $\{p(f)\}$ calculated with the forward transform (Eq. 1) from the manifold of conceivable sets $\{f\}$ are very different from the data p actually observed. The ‘misfit’ is characterized by the parameter χ^2. For uncorrelated noise η of the detector signals and Gaussian distribution with variance σ_i, the likelihood function - the product of the likelihoods of each observation p – becomes $P(p|f,z) \propto \exp\left(-\frac{1}{2}\chi^2\right)$, where $\chi^2 = \sum_{i}^{N_d} \left(\frac{p_i - p_i(f)}{\sigma_i}\right)^2$. Provided α is known, the reconstruction with the largest posterior probability (Eq. (2)) corresponds to the maximum of $\Psi(\alpha, f) = \alpha \cdot S - \frac{1}{2}\chi^2$; α can be interpreted as a regularization parameter which controls the balance between prior information (default model), represented by the entropy term, and data constraints, represented by the misfit parameter χ^2.

The maximization of Ψ with respect to α can be obtained introducing Lagrangean multipliers, which strongly reduce the computational effort. We used the procedure described in Ref. 5. The space of the variables is enlarged to $\{f_i \mid i = 1,2,...,N_p\} \cup \{P_k \mid k = 1,2,...,N_d\}$ but the number of unknowns is reduced from Np to Nd. The equation:

$$\Psi'(\alpha, f, p) = \alpha S - \frac{1}{2}\sum_k \frac{(p_k - P_k)^2}{\sigma_k^2} \tag{5}$$

subject to the constraints $P_k = p_k(f_k)$, is maximized. This leads to an unconstrained maximization of:

$$\tilde{\Psi}(\alpha, f, P) = \alpha S - \frac{1}{2}\sum_k \frac{(p_k - P_k)^2}{\sigma_k^2} + \alpha \sum_k \lambda_k [P_k - p_k(f)] \tag{6}$$

with respect to f, P and λ. Maximizing with respect to f gives the Euler-Lagrange equation:

$$f_i = m_i \exp\left(-\sum_k w_{ik}\lambda_k\right) \tag{7}$$

which constitutes an N_d dimensional basis for possible reconstruction of f. The required Lagrange parameters, λ_k, could be found after maximizing $\tilde{\Psi}$ with respect to λ and P, which amounts to solving the nonlinear equation for λ:

$$\Psi_k(\lambda) = p_k - \sum_{i}^{N_p} I_{ki} m_i \exp\left(-\sum_{k'} I_{k'i}\lambda_{k'}\right) + \alpha\sigma^2\lambda_k = 0 \tag{8}$$

The Jacobian $J_{kk'} = \partial\Psi / \partial\lambda_{k'}$ of the expression is $J_{kk'} = \alpha\sigma_k^2\delta_{ll'} + \sum_k I_{ki}I_{k'i}f_i$ and is strictly positive. So Eq. (13) has a unique solution and can be efficiently solved by the Newton–Raphson method.

Therefore the retrieval of the unknown image f implies the maximization of expression (8) with respect with the Lagrange multipliers λ. After finding the parameters λ. the image can be obtained using Eq. (7). As the maximization does not manipulate directly the unknown image f, smoothing can be applied straightforward only at the end of the iterative process. This has a limited effect and does not improve enough the quality of the reconstruction, especially for distributions with complicated shapes. ME algorithm may produce noisy reconstruction results compared with other kinds of reconstruction algorithms due to the absence of correlation among adjacent pixels. Kim et al. [5] replaced the flat model m with the directly inverted model, obtained by inverting the weight matrix using the singular value decomposition (SVD) technique. The SVD-based initial guess of the reconstruction allows the adjacent pixels to link smoothly. This technique succeeds in enhancing the reliability of the algorithm and improves the quality of the reconstruction for a geometry with 16 projections and 192 bins in each projection. However for the JET geometry (2 projections with a total of 19 projection bins), which determines the highly indeterminacy of the tomographic problem, the directly inverted model is far from the desired solution. This may lead to a local solution during the maximization of $\tilde{\Psi}(\alpha, f, P)$ (Eq. 6). Therefore we used a multiple run procedure. We start with a flat model $m = const$. The smoothing procedure was applied after each full run of the ME algorithm (solving Eq. 8). Then the reconstructed image was used, in a new run, as a default model, replacing the flat one. This procedure improves the robustness of the algorithm and the quality of the reconstruction.

2.2.4 Tikhonov regularization

The Tikhonov regularization is one of the most well-known form of regularization techniques for ill-posed problems. Assuming a matricial form of Eq. 1: $W \cdot f = p$, the Tikhonov regularization technique is seeking for a solution f, defined as the minimizer of the following weighted combination of the residual norm $\|W \cdot f - p\|^2$ and the 2-norm $\|L(f)\|^2$, where the matrix L is typically either the identity matrix I or a discrete approximation of the derivative operator (usually the first or second order derivative operator):

$$\Psi(f) = \|W \cdot f - p\|^2 + \lambda \cdot \|L(f)\|^2 = MIN \tag{9}$$

λ is a regularization parameter. It controls the weight given to minimization of the side constraint relative to minimization of the residual norm; λ also controls the sensitivity of the regularized solution f, to perturbations in W and p, and the perturbation bound is proportional to λ^{-1}.

Several choices of the operator L were reported. Second order linear regularization $L = \nabla^2$, where ∇^2 is the Laplacian operator in two dimensions, is reviewed in Ref. 7. The gradient is minimized if first order linear regularization is chosen [see Ref. 7] $L(f) = \|f_x^{'}\|^2 + \|f_y^{'}\|^2$ (where $f_x^{'}$ and $f_y^{'}$ are the partial derivatives with respect to x and y. $L(f) = \sum_i \frac{(f_i')^2}{f_i}$ in case of Fisher information reconstruction algorithm [see Ref. 8], which can be viewed as belonging also to the class of Tikhonov regularization methods. The minimization of $\|L(f)\|$ introduces different intrinsic smoothing principle in the algorithm, depending on the particular choice of L. $\|L(f)\|^2$ control the smoothness of the regularized solution, depending on the particular choice of L. Second order regularization selects the solution with least curvature. First order regularization minimizes the roughness of the reconstruction. Minimum Fisher information is essentially a smoothening principle just like linear regularization. The low value regions of f are more strongly smoothed, whereas smoothing is less pronounced where f is high and therefore more reliable. In our approach we used $L = I$, where I is the identity matrix. Therefore the norm of the solution is minimized together with the residual norm (Eq. 9). The smoothing effect is the one typically associated with a square integrable kernel. However, this intrinsic smoothing, not connected with the magnetic information, is insufficient to avoid global distortions in the reconstruction, generated by the limited experimental information. Therefore we used additional smoothing - median filtering smoothing on flux surfaces and projection resampling - as described previously.

For solving (9) we used the method based on filter factors and the singular value decomposition (SVD). The method can be briefly described as follows. The general solution f_{reg} of the regularization problem can be written in the form [9]:

$$f = \sum_i \eta_i \frac{u_i^T p}{s_i} v_i, \quad \text{where } W = USV^T = \sum_k u_k s_k v_k^T \tag{10}$$

and η_i are filter factors for the particular regularization method. The filter factors must have the important property that as s_i decreases, the corresponding η_i tends to zero in such a way that the contributions $\left(u_i^T p / s_i\right) f_i$ to the solution from the smaller s_i are effectively filtered out [10]. Otherwise the solution is dominated by the terms in the sum corresponding to the smallest s_i. As a consequence, the solution has many sign changes and thus appears completely random. The difference between the various regularization methods lies essentially in the way that these filter factors η_i are defined. It can be shown that for Tikhonov regularization with $L = I$ filter factors are: $\eta_i = \frac{s_i}{\left(s_i^2 + \lambda^2\right)}$ and the filtering effectively sets in for $s_i < \lambda$. The algorithm is complete if a method for choosing the regularization parameter λ is defined. The regularization parameter was chosen such that the residual norm for the regularized solution satisfies:

$$\|W \cdot f - p\| = \|\eta\| \tag{11}$$

where η is a good estimation of the noise accompanying the experimental data. An underestimate of $\|\eta\|$ is likely to produce an under-regularized solution with a very large norm while, on the other hand, an overestimate produces an over-regularized solution with too large regularization error.

2.2.4 Monte Carlo back-projection technique

This algorithm starts from an empty image $f_i = 0$. Then, mathematically "grains" of fixed intensities do are randomly allocated. The l-th grain is accepted in pixel i and therefore f_i is increased with the quantity do if, for all corresponding projections p_k, the following inequality is valid: $p_k - \left(f_i - do\right) w_{ik} \geq 0$. The restored object is built up by such successive successful allocations. In order to generate the position where we try to allocate the grain, for the two available projections, $p^{horiz}_{k\{k=1..10\}}$ and $p^{vert}_{k\{k=11..19\}}$ two random numbers, k^{horiz} and k^{vert} , respectively, are generated. These two numbers select two projection rays and their intersection defines the point where we attempt to allocate the grain. A uniform generation of k^{horiz} and k^{vert} has no connection with the experimental available data. So it is more efficient to generate the two random numbers using $p^{horiz}_{k\{k=1..10\}}$ and $p^{vert}_{k\{k=11..19\}}$ as probability distribution functions. k^{horiz} and k^{vert} will be distributed preferentially where the cumulative sum $cumsum = \sum_k p_k$ has a higher slope and p_k reaches a local maximum. The generation of grain position by a procedure sensitive to the experimental data increases the speed of the reconstruction process. The magnitude of the quantity do is important for proper results. Building the image f with big grains will not allow the calculated projections $p^{calc}_k = \sum_i f_i w_{ik}$ to be more than a coarse approximation of the experimental projections p^{calc}_k because of residuals. Obviously, the use of small grains will increase the computation time.

3. Results and discussion

The efficiency of each method has been tested using phantoms with shapes characteristic of JET neutron/gamma tomography and representative results are presented in Fig. 1. Each row corresponds to a phantom and its reconstruction - from left to right: the phantom and the ML, ME, TR, and MCBP reconstructions. The virtual magnetic contour lines used for reconstruction are superimposed on each image.

The peak and hollow phantom are the most frequent distribution shapes encountered in experiments. However for a full characterization of the methods, more complicated shapes must be taken into account. Neutron emissivity profiles in case of DT experiments provide several challenging shapes for tomographic reconstruction. Three such shapes were used here: “banana”, symmetrically reversed “banana” and peak plus “banana”. The “banana” phantom corresponds to an experiment where the DT-neutron emission was measured in the ohmic deuterium discharge during the off-axis injection of the T neutral beam. The symmetrically reversed “banana” phantom is, from the tomographic point of view, a more difficult case. The diverging lines of sight corresponding to the horizontal camera are more widely spread in the "banana" region on the high field side and this results in a reduced information density leading to shadow effects: there are more possibilities in this region to distribute each detector signal among different cells than in the region close to the detectors and this may result in reduced spatial resolution. The peak plus “banana” phantom corresponds also to a DT experiment, where the profile was recorded just after a T-puff, and tritons partly penetrated to the plasma core from the periphery.

Several figures of merit were used in order to complete the qualitative evaluation of the quality of the reconstruction with a quantitative one. A global evaluation of the reconstruction is given by the correlation coefficient which gives a comparison between the phantom f^{ph} and the reconstruction f^{rec}. This factor has the value 1 for an ideal reconstruction.

The ratio R_{emiss} between the total volume of the distribution given by the tomographic reconstruction method and the total volume of the phantom may assess the correctness of the total emissivity reconstruction, also by means of a single number.

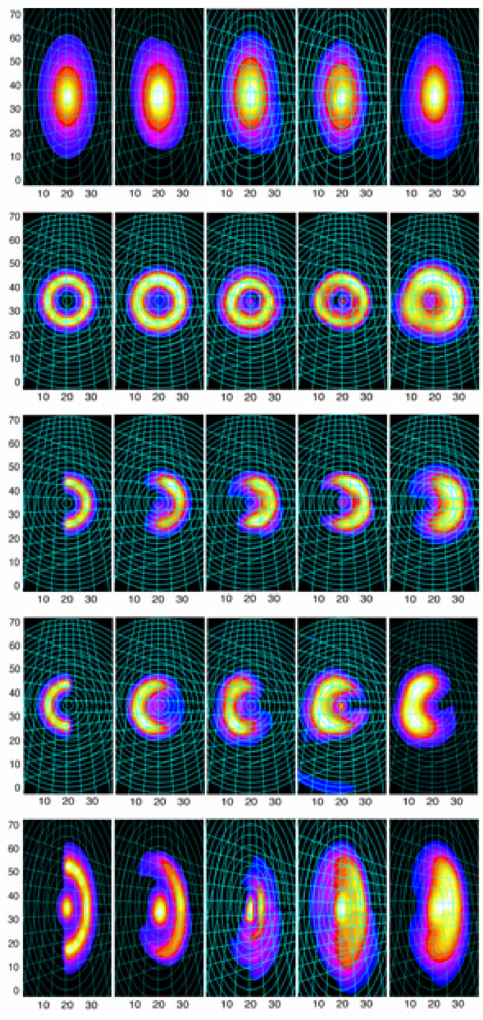

Figure 1 – The test phantoms and their reconstruction. Each row corresponds to a phantom - from top to bottom: peak, hollow, "banana", symmetrically reversed "banana" and peak plus "banana". The first column corresponds to the phantom image, the other columns correspond to reconstructions obtained using the different methods used in this paper – from left to right: ML, ME, TR, MCBP.

Finally, also a global evaluation is given by the comparison between the initial projections $p^{(ini)}$ and the calculated ones $p^{(calc)}$; projections $p^{(ini)}$ were calculated using Eq. 1, where f is the phantom; projections $p^{(calc)}$ were calculated using the same equation, but in this case f represents the reconstruction. This comparison must be taken into account cautiously.

For a good reconstruction a good agreement must exists between $p^{(ini)}$ and $p^{(calc)}$. However, since a limited set of projections is available, a good agreement does not guarantee necessarily a good reconstruction.

The assessment of the spatial resolution can be obtained by means of line profiles. The horizontal and vertical line profiles describe the image intensity variation along the horizontal and vertical axes of a coordinate system with the origin in the centre of the image. The main image features, for all the phantoms, intersect these two axes.

Information about the quality of the shape and size reconstruction is given by line integrals, calculated along the magnetic contour lines, starting from the centre of the reconstruction and covering the whole image.

The values obtained for the correlation coefficient $corr$ and the ratio R_{emiss} describing the reconstruction of the total emissivity are given in Table 1 and 2, respectively. The other figures of merit, which allow a graphical representation, are illustrated in Fig. 2-3.

Table 1 - The correlation coefficient $corr$.

Phantom	Reconstruction method			
	ML	ME	TR	MCBP
peak	0.993	0.990	0.989	0.996
hollow	0.961	0.949	0.951	0.870
"banana"	0.935	0.931	0.908	0.857
symmetrically reversed "banana"	0.875	0.861	0.836	0.832
peak plus "banana"	0.874	0.667	0.837	0.844

Table 2 - The ratio of reconstructed volumes R_{emiss}.

Phantom	Reconstruction method			
	ML	ME	TR	MCBP
peak	1.07	1.27	0.98	1.01
hollow	1.23	1.28	1.05	2.05
“banana”	1.30	1.56	1.64	1.85
symmetrically reversed “banana”	1.45	1.59	1.76	1.93
peak plus “banana”	0.86	0.75	1.44	1.86

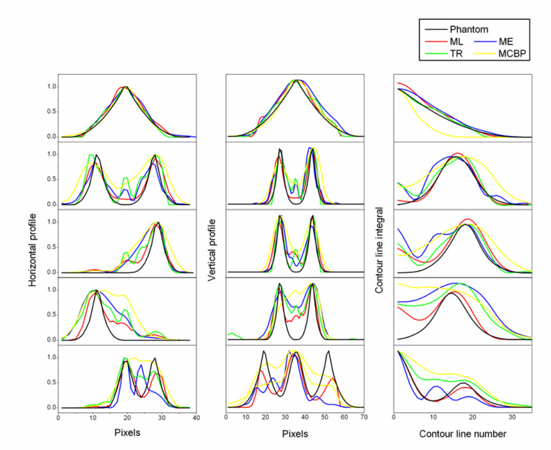

Figure 3 – Figures of merit; each row corresponds to a phantom – from top to bottom: peak, hollow, “banana”, symmetrically reversed “banana”, peak plus “banana”; each column corresponds to a specific figure of merit – from left to right: horizontal line profile, vertical line profile, integrals along magnetic contour lines.

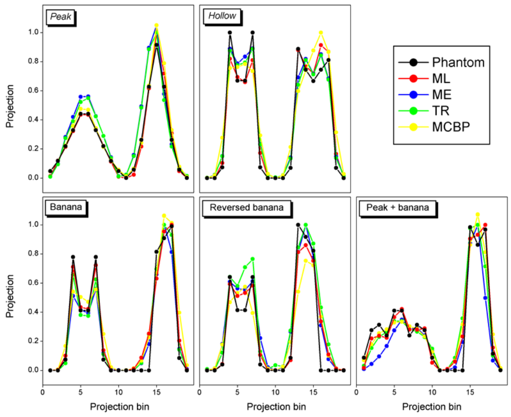

Figure 4 – Projections calculated using the phantom and the reconstruction, respectively: peak (top-left), hollow (top-right), “banana” (bottom-left), symmetrically reversed “banana” (bottom-middle), peak plus “banana” (bottom-right).

For the peak phantom, the most common distribution encountered in experiments, good reconstructions are obtained using all the methods. The ML method gives the best value for the root mean square difference between projections calculated using the phantom and the reconstruction. The TR method offers optimal results for the line profiles. The correlation coefficient and the ratio of reconstructed volumes finest results are provided by the MCBP. In fact, all the methods give accurate results, with similar values for all factors of merit. Similar remarks are valid also for the case of the hollow phantom with the exception of the MCBP method, which gives a reconstruction with lower spatial resolution. Finest results are obtained using the ML method except the ratio of reconstructed volumes for which the TR method gives the result closest to 1. It must be noticed that the ML method provides, for this distribution and also for the next ones, the most regular and symmetric shapes.

The methods give significantly different results when the symmetry of the distribution, with respect to the two axes, is reduced or eliminated. The line profiles (both horizontal and vertical), but especially the contour line integral values proves that the best results, in case of “banana” and symmetrically reversed “banana” are obtained using the ML method. As far as the other methods are concerned, it is difficult to choose between the TR and ME methods. The images show more similarity between the shapes reconstructed by the ME method and the phantoms. This is confirmed also by the values of the correlation coefficient. The images retrieved using the TR method are slightly distorted and affected by a central artefact. However, the TR method gives better values for the line profiles (both horizontal and vertical), and also for the contour line integral. But starting with the "banana" phantom, the TR method does not provide the best values for R_{emiss} anymore. The MCBP method is able to reproduce the "banana" shapes but with the same low spatial resolution. The peak plus "banana" distribution is, from the tomographic point of view, the most complex and challenging structure. The only reasonable reconstruction is given by the ML method. The TR method looses spatial resolution and almost equals the MCBP method. Both methods prove unable to completely resolve the two features in the image. The ME method discriminates the two components in the image, but introduces shadow artefacts in retrieving the "banana" component which is also shifted and reproduced incompletely. The hierarchy of the methods is confirmed by the quality factors.

The reconstruction time is an important parameter especially if the method is intended to be used in inter-shot analysis. The TR method is the fastest one (0.8 min), due to its formulation which involves pure matrix manipulation. Most of the computer time needed for this method is spent on smoothing. However, smoothing can not be avoided in order to obtain as correct as possible reconstruction. The computing time for the ML (3.5 min) is still practicable for inter-shot analysis. The computing time is reported for a MATLAB implementation.

The results of the comparative study concerning the assessment of the quality of the tomographic methods for reconstruction of neutron and gamma emissivity was published [11].

The package of methods was used during the JET experimental campaigns. Diagnostics support, consisting in the reconstruction of the gamma emissivity distribution, was provided for fast ion studies. Typical reconstructions obtained JET experimental campaigns are presented in Fig. 5. The results obtained during experiments contributed to two publications [12-13].

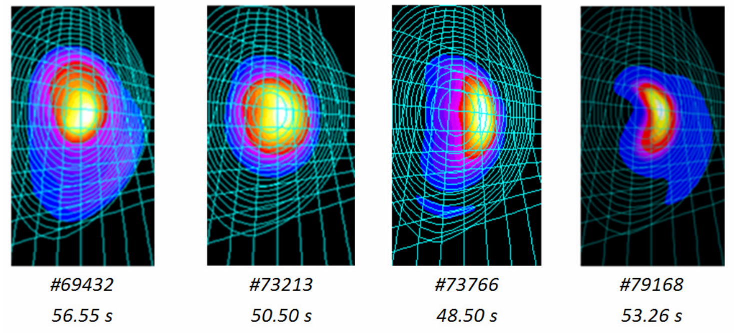

Figure 5 – Typical reconstructions of the gamma emissivity distributions

4. Conclusion

In conclusion we can say that the comparative evaluation of the tomographic methods is able to establish a clear hierarchy of the tested methods. The evaluation has been performed with phantoms. These numerically simulated emissive distributions are characteristic for JET neutron and gamma tomography. They cover most of the range of possible distributions for this kind of tomography. Simple but frequent shapes are considered together with the retrieval of sophisticated structure in the emissive distribution which proved to be essential for a complete image of the quality and reliability of the methods. The evaluation reveals that the ML method is the only one able to encompass the reconstruction, with a good quality, of all structures of the emissive distribution. The ML method provides the finest results in terms of shapes reconstruction and resolution and produces artefact free images. For the simple shapes (peak and "banana"), the total emissive volume is better retrieved by the TR method. This can be explained by means of the effects of the smoothing, which determines a blurring effect, superimposed on the image. The effect is stronger in case of the ML method where the amount of smoothing is increased: the smoothing operator is applied at each iteration, while for the TR method smoothing is applied only once, after the reconstruction. However, for more complicated shapes, the larger amount of smoothing becomes an advantage because it drives the reconstruction closer to the shapes to be recovered. For simple, but frequent experimental type of distributions (peak, hollow), all the methods provide good results. For this cases, if very fast reconstructions are needed (e.g. for a large amount of data processing), the TR method is an appropriate choice. The package of methods was used in order to provide support in JET experimental campaigns. It allowed the retrieval of useful information needed during the experiment.

Acknowledgement
The reported work includes contributions from the following people outside the EUATOM-MEdC Association: Georges Bonheure (Partners in the TEC , 'Euratom-Belgian state' Association LPP-ERM/KMS, B 1000 Brussels, Belgium), Vasily Kiptily (EURATOM/UKAEA Association, Culham Science Centre, Abingdon, Oxon, UK), Andrea Murari (Consorzio RFX, Associazione ENEA-Euratom per la Fusione, Padova, Italy).

References

[1] T. Craciunescu, G. Bonheure, V. Kiptily, A. Murari, S. Soare, I. Tiseanu, V. Zoita, Nuclear Inst. and Methods in Physics Research, A, 595, p. 623–630, 2008.
[2] L.A. Shepp, Y. Vardi, IEEE Transactions on Medical Imaging, Vol. 1 (1982) 113 121.
[3] K. Lange, R. Carson, JCAT vol. 8 (1984) 306-316.
[4] J. Skilling, in: P.F. Fougère (Ed.), Maximum Entropy and Bayesian Methods, Kluwer Academic Publishers, Dordrecht (1990) pp. 341 350.
[5] J. Kim, W. Choe, Review of Scientific Instruments 77, 023506-1-6, 2006.
[6] N. Iwama, H. Yoshida, H. Takimoto, Y. Shen, S. Takamura, and T. Tsukishima, Appl. Phys. Lett. 54, 502-504, 1989.
[7] A.K. Chattopadhyay, C.V.S. Rao, Review Of Scientific Instruments 76, 063502 (2005).
[8] M. Anton, H. Weisen, M.J. Dutch, W. von der Linden, F. Buhlmann, R. Chavan, B. Marletaz, P. Marmillod and P. Paris, Plasma Phys. Control. Fusion 38, 1849–1878. (1996)
[9] P. Hansen, Numer. Algo. 46 (2007), pp. 189-194.
[10] P. Hansen, Numer. Algorithms 46 (2007) 189.
[11] T. Craciunescu, G. Bonheure, V. Kiptily, A. Murari, I. Tiseanu, V. Zoita, Nuclear Inst. and Methods in Physics Research, A, 605, pp. 373-384, 2009
[12] V.G. Kiptily, F.E. Cecil, O.N. Jarvis, M.J. Mantsinen, S.E. Sharapov, L. Bertalot, S. Conroy, L.C. Ingesson, T. Johnson, K.D. Lawson, S. Popovichev, Nucl. Fusion 42(2002) 999-1007
[13] V.G. Kiptily, I.N. Chugunov, D.B. Gin, A.E. Shevelev, P.J.L. Heesterman, A. Murari3, 33rd EPS Conf. on Plasma Physics (Rome, Italy, 19–23 June 2006) vol 30I(ECA) P1.077.
[14] V. G. Kiptily, C. P. Perez von Thun, S. D. Pinches, S. E. Sharapov, D. Borba, F. E. Cecil, D. Darrow, V. Goloborod'ko, T. Craciunescu, T. Johnson, F. Nabais, M. Reich, A. Salmi, V. Yavorskij, M. Cecconello, G. Gorini, P. Lomas, A. Murari, V. Parail , S. Popovichev, G. Saibene, R. Sartori, D.B. Syme, M. Tardocchi, P. de Vries, V.L. Zoita. Recent progress in fast ion studies on JET. Nuclear Fusion, 49, p. 065030, 2009.
[15] V.G. Kiptily, G. Gorini, I. Proverbio, M. Tardocchi, I.N. Chugunov, D. Gin, M. Nocente, S.D. Pinches, S.E. Sharapov, A.E. Shevelev, T. Craciunescu, F.E. Cecil, M. Gatu Johnson, V. Goloborod'ko, C. Hellesen, T. Johnson, K. Kneupner, A. Murari, P.G. Sanchez, D.B. Syme, P. de Vries, V. Yavorskij, V.L. Zoita. Doppler Broadening of Gamma Ray Lines and Fast Ion Distribution in JET plasmas, 11th IAEA Technical Meeting on Energetic Particles in Magnetic Confinement Systems, Kyiv, Ukraine.